RSC Advances

PAPER

View Article Online
View Journal | View Issue

Cite this: *RSC Adv.*, 2019, **9**, 18978

Controlled degradation of low-fouling poly(oligo(ethylene glycol)methyl ether methacrylate) hydrogels†

Muhammad M. Shoaib,[a] Vincent Huynh,[a] Yousuf Shad,[a] Rashik Ahmed,[b] Alexander H. Jesmer,[a] Giuseppe Melacini[ab] and Ryan G. Wylie[*ac]

Received 8th May 2019
Accepted 10th June 2019

DOI: 10.1039/c9ra03441b

rsc.li/rsc-advances

Degradable low-fouling hydrogels are ideal vehicles for drug and cell delivery. For each application, hydrogel degradation rate must be re-optimized for maximum therapeutic benefit. We developed a method to rapidly and predictably tune degradation rates of low-fouling poly(oligo(ethylene glycol) methyl ether methacrylate) (P(EG)$_x$MA) hydrogels by modifying two interdependent variables: (1) base-catalysed crosslink degradation kinetics, dependent on crosslinker electronics (electron withdrawing groups (EWGs)); and, (2) polymer hydration, dependent on the molecular weight (M_W) of poly(ethylene glycol) (PEG) pendant groups. By controlling PEG M_W and EWG strength, P(EG)$_x$MA hydrogels were tuned to degrade over 6 to 52 d. A 6-member P(EG)$_x$MA copolymer library yielded slow and fast degrading low-fouling hydrogels suitable for short- and long-term delivery applications. The degradation mechanism was also applied to RGD-functionalized poly(carboxybetaine methacrylamide) (PCBMAA) hydrogels to achieve slow (~50 d) and fast (~13 d) degrading low-fouling, bioactive hydrogels.

1. Introduction

Degradable low-fouling hydrogels are being developed as implantable vehicles for drug and cell delivery to decrease the incidence rate of adverse events (*e.g.* foreign body response (FBR)) by minimizing non-specific protein adsorption and cell binding.[1,2] The FBR cascade impedes drug release or cell egress from hydrogels by surrounding implants in dense fibrous capsules.[3] Due to their strong hydration shells, non-specific protein adhesion to low-fouling polymers such as poly(oligo(ethylene glycol)$_x$methyl ether methacrylate) (P(EG)$_x$MA) and poly-(carboxybetaine methacrylamide) (PCBMAA) is energetically unfavorable.[4] P(EG)$_{4-5}$MA coated surfaces resist protein fouling[5] and platelet binding.[6] Moreover, carboxybetaine coated surfaces have been shown to prevent non-specific protein adsorption in serum[7] and resist the FBR for up to 3 months *in vivo*.[8]

The degradation of low-fouling hydrogels must be tuned to match requirements for short- and long-term delivery applications. Hydrogel drug delivery applications, such as cancer therapies,[9–11] wound healing,[12] pain management,[13,14] and retinal degenerative disease treatments,[15,16] often require drug release profiles that span a wide-distribution of time-frames, ranging from as little as a days to several weeks. We therefore require low-fouling hydrogels with highly tunable degradation timeframes. Predictable degradation rates are particularly important for long-term drug delivery (~4 weeks) wherein uncontrolled hydrogel degradation can limit efficacy by increasing the initial burst release.[17] Thus far, degradation mechanisms for low-fouling gels have focused on endogenous triggers (*e.g.* reduction of disulfide bonds,[18–20] enzyme cleavage sites[21]), or hydrolytic bonds (*e.g.* esters, hydrazones).[22] *In situ* crosslinking P(EG)$_x$MA copolymers with aldehyde and hydrazide repeats yield hydrogels that crosslink through reversible hydrazone bonds with degradation rates proportional to pH and copolymer molecular weight (M_W).[23,24] Carboxybetaine copolymers with zwitterionic thiol repeats have been developed to achieve biodegradable hydrogels in the presence of reducing agents such as glutathione.[19,20,25] A detailed description of hydrogel degradation mechanisms is provided in the referenced review.[26]

Endogenous triggered degradation is dependent on dynamic biological environments, which may result in unpredictable degradation rates, and current methods to tune hydrolysis rates require extensive synthetic modifications. To improve therapies requiring low-fouling hydrogels, there is a great need to develop a versatile method to easily tune degradation rates that are independent of endogenous

[a]*Department of Chemistry and Chemical Biology, McMaster University, Hamilton, Ontario, L8S 4M1, Canada. E-mail: wylier@mcmaster.ca*

[b]*Department of Biochemistry and Biomedical Sciences, McMaster University, Hamilton, Ontario, L8S 4M1, Canada*

[c]*School of Biomedical Engineering, McMaster University, Hamilton, Ontario, L8S 4M1, Canada*

† Electronic supplementary information (ESI) available. See DOI: 10.1039/c9ra03441b

triggers and don't require additional synthetic steps. To achieve an accessible library of low-fouling hydrogels with varied degradation profiles, hydrogels should be formed by simply mixing a limited number of pre-defined polymers for *in situ* crosslinking. The combination of low-fouling P(EG)$_x$MA hydrogels of varying hydration levels with different crosslinkers for irreversible base-catalyzed degradation[27,28] is expected to provide a method to rapidly tune degradation over clinically relevant timeframes. Irreversible base-catalyzed crosslink degradation[27,28] is solely dependent on the pH of the implantation site, a known value, and not reliant on dynamic endogenous triggers. Furthermore, hydrogels composed of P(EG)$_x$MA with different PEG pendant group molecular weights (M_Ws) will exhibit different hydration levels to further tune base-catalyzed crosslinker degradation rates.[29] By simply mixing pre-defined polymers, a library of P(EG)$_x$MA copolymers is expected to yield low-fouling hydrogels with highly tunable degradation kinetics.

2. Materials and methods

2.1 Materials

Triethylene glycol methyl ether methacrylate 93% ((EG)$_3$MA), poly(ethylene glycol)methyl ether methacrylate number average molecular weight (M_n) 300 ((EG)$_{4-5}$MA), poly(ethylene glycol) methyl ether methacrylate average M_n 500 ((EG)$_{8-9}$MA), 4-cyano-4-(phenylcarbonothioylthio)pentanoic acid (CTP), 4,4′-azobis(4-cyanovaleric acid) (V-501), *N*-[3-(dimethylamino)propyl]-methacrylamide (DMAPMA), *t*-butyl bromoacetate, trifluoroacetic acid, 6-chloro-1-hexanol, sodium azide, trichloroisocyanuric acid, TEMPO, sodium bicarbonate, 1.6 M *n*-butyllithium in hexane, 4-(methylsulfonyl)toluene, pyridine, triphosgene, *N*-hydroxysuccinimide (NHS), fluorescamine, triethylamine, picrylsulfonic acid 5% (w/v), sodium dodecyl sulfate (SDS), bovine serum albumin (BSA), and fluorescein sodium salt were purchased from Sigma-Aldrich (Oakville, ON). *N*-(3-Dimethylaminopropyl)-*N*′-ethylcarbodiimide hydrochloride (EDC) was purchased from Chem-Impex International (Wood Dale, IL). 4-Chlorophenyl methyl sulfone was purchased from Alfa Aesar (Ward Hill, MA). *N*-(3-Aminopropyl)methacrylamide hydrochloride, >98% (APMA) was purchased from Polysciences, Inc. (Warrington, PA). 1,2-Bis(2-(4,5-dihydro-1*H*-imidazol-2-yl) propan-2-yl)diazene dihydrochloride (VA-044) was purchased from Toronto Research Chemicals (Toronto, ON). CGRGDS >95% was purchased from GenScript (Piscataway, NJ). Calcein AM fluorescent dye was purchased from Corning, New York, USA. PrestoBlue™ cell viability reagent, Hoechst 33342, HyClone™ calf bovine serum (CBS) and DMEM/F12 1 : 1 were purchased from Thermo Fisher Scientific (Whitby, ON). Methylcellulose (MC; METOLOSE® SM-4000) was purchased from Shin-Etsu Corp (Tokyo, Japan). Solvents were reagent grade and obtained from Caledon Laboratories (Georgetown, ON) and Thermo Fisher Scientific (Whitby, ON). Dibenzylcyclooctyne-NHS ester (DBCO-NHS) was gifted by Dr Alex Adronov at McMaster University (Hamilton, ON).

2.2 Synthesis and characterization of P(EG)$_x$MA copolymers

2.2.1 Synthesis of P(EG)$_x$MA copolymers with *N*-(3-aminopropyl)methacrylamide (P(EG)$_x$MA–APMA). Inhibitors were removed from (EG)$_x$MA monomers using an aluminum oxide column. For P(EG)$_3$MA–APMA, (EG)$_3$MA (2 g, 8.6 mmol), APMA (81.0 mg, 0.44 mmol), CTP (5.8 mg, 21 μmol), and VA-044 (1.35 mg, 4.18 μmol) were dissolved in 2 : 1 water : dioxane (7 mL). For P(EG)$_{4-5}$MA–APMA, (EG)$_{4-5}$MA (1 g, 3.3 mmol), APMA (48 mg, 0.27 μmol), CTP (5.8 mg, 21 μmol) and VA-044 (1.35 mg, 4.2 μmol) were dissolved in 2 : 1 water : dioxane (2.5 mL). For P(EG)$_{8-9}$MA–APMA, (EG)$_{8-9}$MA (1 g, 2 mmol) APMA (29 mg, 0.16 mmol), CTP (5.8 mg, 21 μmol) and VA-044 (1.35 mg, 4.2 μmol) were dissolved in 2 : 1 water : dioxane (1.1 mL). All reaction solutions were freeze–pump–thawed with a nitrogen backfill (3 times), and acidified to pH ∼ 3.5 using 0.1 M HCl prior to polymerization at 40 °C for ∼16 h. Polymers were purified by dialysis (MWCO 12–14k) against pH 3 water and lyophilized to yield a pink paste (P(EG)$_3$MA–APMA: 1.325; P(EG)$_{4-5}$MA–APMA: 0.904; P(EG)$_{8-9}$MA–APMA: 0.948 g).

2.2.2 Characterization of P(EG)$_x$MA–APMA copolymers. Molecular weights (M_W, M_n) and polymer dispersity ($Đ$) of copolymers were determined using an Agilent 1260 Infinity II gel permeation chromatography (GPC) system equipped with an Agilent 1260 Infinity refractive index detector and GE healthcare Superose™ 6 Increase 10/30 GL column in 10 mM PBS running buffer. The column was calibrated with polyethylene glycol (PEG) standards (M_n of 3 to 60 kDa). ^{1}H NMR (600 MHz, D_2O, 128 scans) of P(EG)$_x$MA–APMA and PCBMAA–APMA copolymers determined polymer APMA mole fractions by comparing the intensity of methylene peaks in each repeat unit (Fig. S1–S3†).

2.2.3 Synthesis of P(EG)$_x$MA-azide (P(EG)$_x$MA–AZ) and P(EG)$_x$MA–DBCO copolymers. NHS-AZ derivatives were synthesized as previously described,[27] see ESI† for detailed protocols. P(EG)$_x$MA–APMA polymers were dissolved at 100 mg mL^{-1} in dry DMSO and reacted with NHS-AZ derivatives or NHS-DBCO (1.2 eq. relative to amino groups) and triethylamine (3 eq.) overnight at room temperature. Complete amine consumption was confirmed by ^{1}H NMR (Fig. S4–S15†) and a fluorescamine assay. Polymers were purified by dialysis (MWCO 12–14k) against water at pH ∼ 3 and lyophilized to yield pink pastes. As seen in Scheme 1, three different P(EG)$_x$MA–AZs copolymers were prepared that contained a non-degradable (R1; H), slow-degrading (R2; 4-methylphenyl sulfone), or fast-degrading (R3; 4-chlorophenyl sulfone) carbamate bond for base-catalysed crosslink degradation.

2.2.4 Characterization of P(EG)$_x$MA–AZ and P(EG)$_x$MA–DBCO copolymers. Copolymer cytotoxicity was assessed using NIH 3T3 mouse fibroblasts. Cells in DMEM/F12 media with 10% CBS were seeded in a 96 well plate at 5000 cells per well. Polymer solutions in PBS (sterilized using a 0.2 μm filter) were added to reach a final polymer concentration of 1 mg mL^{-1}. Cells were incubated at 37 °C, 5% CO_2 for 24 h. PrestoBlue reagent solution (22 μL) was then added to each well and incubated at 37 °C, 5% CO_2 for 15 min. Fluorescence was measured using a BioTek Cytation 5 plate reader (λ_{ex} = 560 nm; λ_{em} = 590 nm). Copolymer lower critical solutions temperatures

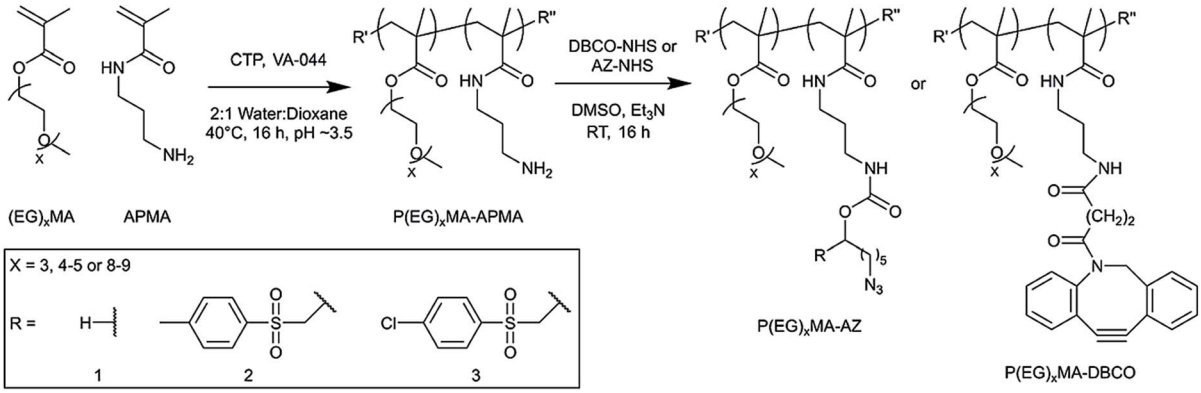

Scheme 1 Synthesis of P(EG)$_x$MA–AZ and P(EG)$_x$MA–DBCO copolymers for *in situ* crosslinking. P(EG)$_x$MA–APMA copolymers were synthesized by RAFT polymerization for subsequent derivatization with NHS-AZ derivatives or NHS-DBCO. For each PEG M_W, three different P(EG)$_x$MA–AZ copolymers were synthesized with a non-degradable crosslinker (R1 = H), and two degradable crosslinkers with EWGs (R2 = 4-methylpheyl sulfone, and R3 = 4-chlorophenyl sulfone).

(LCSTs) were determined by following the absorbance (600 nm) of polymer solutions (25 mg mL^{-1}) in pH 7.4 PBS or pH 9.3 0.1 M borax buffer in a 96 well plate over a temperature range of 30–65 °C and a ramp of 1 °C per 10 min on a BioTek Cytation 5 plate reader.

2.3 Gelation and characterization of P(EG)$_x$MA hydrogels

Gelation time was measured *via* gravitational flow analysis. Hydrogels (100 μL) were made with equal volumes and concentrations (50 mg mL^{-1}) of azide and DBCO copolymers. Vials were tilted periodically until flow was no longer observed. The number of crosslinks was determined by tracking the absorbance of 100 μL hydrogels (5 wt%) at 309 nm over time to measure consumption of DBCO over the first 24 h; gels were formed in a 96-well polypropylene plate. After 24 h, a 10-fold excess of sodium azide was added to react all remaining DBCO groups to determine background hydrogel absorbance. Hydrogel (5 wt%) cloud points were measured using the same procedure as for copolymer LCSTs.

Hydrogel swelling was determined by incubating 100 μL hydrogels (5 wt%) in pH 7.4 PBS at 37 °C for 22 h. The initial hydrogel wet weight was recorded. After selected time intervals, buffer was removed from hydrogel surfaces and their wet weight was recorded.

2.4 ^{1}H NMR kinetic analysis of P(EG)$_x$MA–AZ–R3 copolymer degradation

^{1}H NMR spectra were recorded at 37 °C with 128 scans, 32 K complex points and spectral widths of 20 ppm on a Bruker 700 MHz spectrometer equipped with a TCI cryoprobe. All spectra were processed and analyzed in TopSpin 3.2.1. The base-catalyzed degradation of the polymers was assessed through the time-dependent increase in the ^{1}H-NMR signal intensity of the nascent hydrolyzed product centred around ~7.8 ppm. For the purpose of comparison, the enhancement in the hydrolyzed product intensity was measured relative to the final intensity of the P(EG)$_{8-9}$MA–AZ–R3 hydrolyzed product at the end of the 3 h period. The resulting experimental points were used to create the kinetic profiles shown in Fig. 3D. The initial hydrolysis rate for P(EG)$_{8-9}$MA–AZ–R3 was determined by linear regression to compute the slope over the first 1 h period. To determine the initial hydrolysis rates of P(EG)$_3$MA–AZ–R3 and P(EG)$_{4-5}$MA–AZ–R3 copolymers, a linear regression was used to compute the slopes over the first 1 h period post lag phase (0.6 h); lag phase is defined as the initial period with no detectable hydrolysis.

2.5 Protein adsorption and cell adhesion on P(EG)$_x$MA hydrogels

2.5.1 Synthesis of BSA-fluorescein and RGD-AZ. For BSA-fluorescein synthesis, EDC (1.45 mg, 7.6 μmol) and NHS (0.87 mg, 7.5 μmol) were added to a fluorescein sodium salt (3.2 mg, 8.5 μmol) solution in 1 mL DMSO and incubated in the dark at room temperature for 25 min. Separately, 100 mg of BSA was dissolved in 9 mL of pH 7.4 PBS and combined with the NHS activated fluorescein solution. The solutions were reacted for 2 h at room temperature in the dark then dialyzed (MWCO 12–14k) against PBS in the dark at 4 °C. For RGD-AZ synthesis, CGRGDS (11 mg, 14 μmol) was dissolved in water (0.1 mL) with triethylamine (7.8 μL, 3 eq.). NHS-AZ (R1; 20 mg, 4 eq.) was dissolved in methanol (0.3 mL) and added to the peptide solution. The solution was reacted overnight at room temperature. The precipitate was collected by centrifugation and washed with water. The solid was dissolved in 0.1 M HCl, and the aqueous layer was washed with DCM (3 times). The aqueous layer was lyophilized to yield a white powder (3 mg). MS (ESI) analysis determined $[M + 1]^+$ peaks of 932.4 g mol^{-1} for disubstituted peptide and 763.4 g mol^{-1} for monosubstituted peptide.

2.5.2 BSA adsorption assay. P(EG)$_x$MA and PCBMAA hydrogels (60 μL, 5 wt%) were formed in triplicate in a 96-well plate and incubated at 37 °C for 5 h. PCBMAA–MC hydrogels were formed by mixing 10 wt% PCBMAA–DBCO dissolved in PBS with 0.5 wt% MC and 10 wt% PCBMAA–AZ–R1 dissolved in PBS with 0.5 wt% MC and gelled for 5 h at 37 °C. After

gelation, BSA-fluorescein (60 μL at 0.5 mg mL^{-1}) was pipette onto gels and incubated at 37 °C for 2 h. The solution on top of the gels was removed and gels were rinsed 3 times with PBS. Gels were immersed in 240 μL of 1× PBS with 0.08 wt% SDS and incubated overnight. The mixture was then sonicated for 30 min to extract residual BSA-fluorescein and the fluorescence was measured using a BioTek Cytation 5 plate reader (λ_{ex} = 494 nm; λ_{em} = 521 nm). The concentration was determined using a BSA-fluorescein calibration curve of known concentrations.

2.5.3 Cell adhesion assays. 60 μL hydrogels (5 wt%) in pH 7.4 PBS were formed in a 96 well plate and allowed to gel for 5 h at 37 °C. RGD-AZ (60 μL, 1 mg mL^{-1} in PBS) was added on top of the hydrogels and incubated overnight at 4 °C. Gels were then immersed in PBS for 2 d at 4 °C to remove unreacted RGD-AZ. 5000 NIH 3T3 mouse fibroblasts in DMEM/F12 with 10% CBS were seeded on top of each hydrogel (with and without RGD-AZ) and incubated for 24 h at 37 °C, 5% CO_2. Cells were then stained with Calcein AM and Hoechst, as per the manufacturer's protocol. Gels were then rinsed with PBS (3 times) to remove non-adhered cells and imaged using a BioTek Cytation 5 cell imager.

3. Results and discussion

We developed low-fouling P(EG)$_x$MA hydrogels with tunable degradation rates by controlling two interdependent variables: (1) base-catalysed crosslink degradation kinetics, dependent on the strength of the incorporated electron withdrawing group (EWG; Fig. 1A); and, (2) polymer hydration, dependent on the M_W of PEG pendant groups (Fig. 1B). By combining P(EG)$_x$MAs with different PEG pendant groups (x = 3, 4–5, and 8–9) with two different crosslinkers (EWG = 4-methylphenyl sulfone or 4-chlorophenyl sulfone), we developed a 6-member copolymer library to rapidly tune P(EG)$_x$MA hydrogel degradation over 6, 13, 31, or 52 d, yielding gels suitable for short- and long-term applications (Fig. 1C). We also demonstrated the degradation of RGD functionalized low-fouling PCBMAA hydrogels over 13 and 52 d to produce bioactive, low-fouling gels for cell delivery applications.

3.1 Synthesis and chemical characterization of P(EG)$_x$MA copolymers

Because P(EG)$_x$MA is synthesized by controlled radical polymerization, monomers with reactive functional groups can be

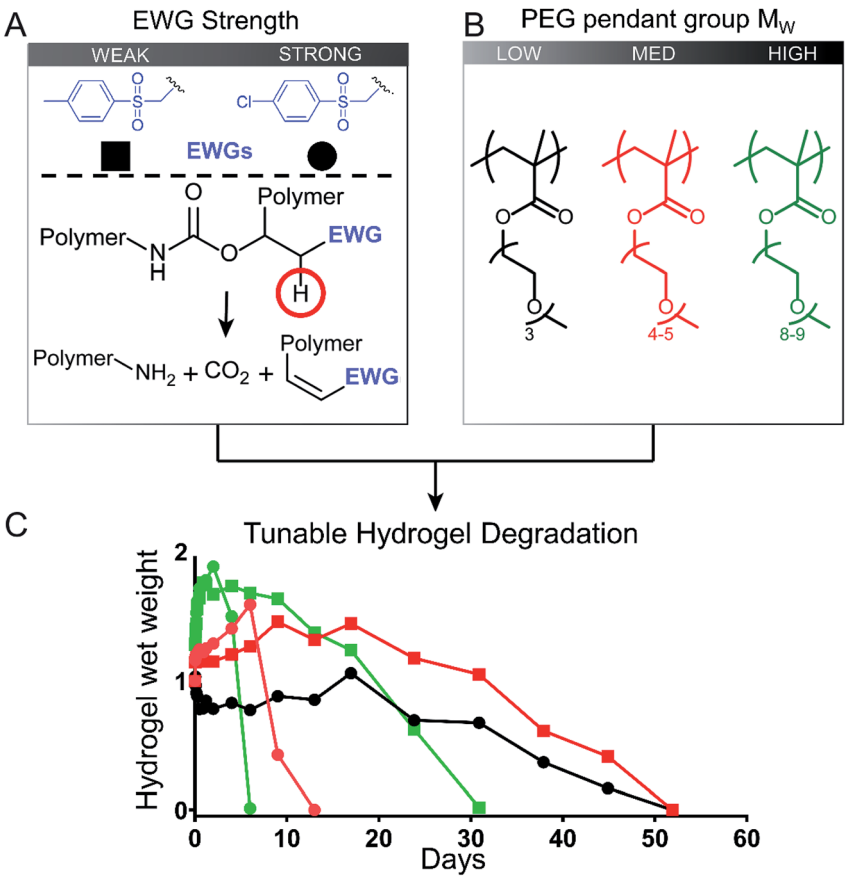

Fig. 1 Schematic highlighting the short- and long-term degradation of low-fouling hydrogels from a library of P(EG)$_x$MA copolymers with two different crosslinkers. (A) Irreversible base-catalyzed hydrolysis of carbamate crosslinks tuned with two different EWGs (4-methylphenyl sulfone and 4-chlorophenyl sulfone). Deprotonation site is highlighted by a red circle. (B) The M_W of PEG pendant groups in P(EG)$_x$MA influenced hydrogel degradation rates. (C) Tunable hydrogel degradation from 6 to 52 days was achieved by creating a library consisting of 3 P(EG)$_x$MA copolymers and two different EWGs. Lower PEG M_W (less hydrated) P(EG)$_x$MAs and weaker EWGs produced slower degradation rates.

polymerized into P(EG)$_x$MA copolymers for *in situ* crosslinking[30] and controlled degradation.[28] We first synthesized random P(EG)$_x$MA copolymers with *N*-(3-aminopropyl)methacrylamide (APMA) using reversible addition–fragmentation chain-transfer (RAFT) polymerization to yield P(EG)$_x$MA–APMA with M_Ws and dispersities ($Đ$) between 30–40 kDa and 1.06 to 1.35, respectively (Scheme 1; Table 1). P(EG)$_x$MA–APMA copolymers with different PEG pendant groups (x = 3, 4–5, and 8–9), were prepared to determine the influence of polymer hydration on hydrogel degradation.

The (EG)$_x$MA to APMA composition in copolymers was optimized to ensure similar crosslink densities (crosslinks per g of polymer) in all P(EG)$_x$MA hydrogels, which allowed for the comparison of polymer hydration on degradation rates. To this end, P(EG)$_3$MA–APMA, P(EG)$_{4-5}$MA–APMA, and P(EG)$_{8-9}$MA–APMA were synthesized with 2, 5 and 10 APMA mol%, respectively, as confirmed by ^{1}H NMR upon comparing integrations of methylene peaks in (EG)$_x$MA and APMA (Table 1; Fig. S1–S3†). Due to sterics associated with PEG pendant groups, greater crosslinker mole fractions, and thus APMA, were required for P(EG)$_x$MAs with higher PEG M_Ws to standardize crosslink density.

P(EG)$_x$MA–APMAs were further functionalized with NHS-AZ molecules resulting in copolymers that contained a non-degradable (R1; H, no EWG), slow-degrading (R2; 4-methylphenyl sulfone), or fast-degrading (R3; 4-chlorophenyl sulfone) carbamate bond for base-catalysed crosslink degradation. Carbamate bond half-lives have been previously reported to vary between 14 h to 437 d by substituting an adjacent EWGs for base-catalyzed degradation.[27] P(EG)$_x$MA–APMAs were also modified with NHS-DBCO to yield P(EG)$_x$MA–DBCO for *in situ* crosslinking with P(EG)$_x$MA–AZ copolymers. All APMA amines were fully reacted with NHS-AZ or NHS-DBCO, as confirmed by ^{1}H NMR (Fig. S4–S15†) and an amine quantification assay (fluorescamine).

To compare polymer hydration through solvation, we studied the solubility of P(EG)$_3$MA and P(EG)$_{4-5}$MA copolymers as a function of temperature and determined LCSTs (Fig. 2, S21A and B†). A homopolymer (HP) of P(EG)$_3$MA had an LCST of 45 °C (25 g L^{-1}), defined as the onset of cloudiness. In comparison to the HP, all P(EG)$_3$MA–AZ and P(EG)$_3$MA–DBCO copolymers demonstrated lower LCSTs near physiological temperature (36–37 °C) due to increased hydrophobic content. The HP of P(EG)$_{4-5}$MA and P(EG)$_{4-5}$MA–AZ copolymers had LCSTs of 62 and 52–54 °C, respectively. Interestingly, P(EG)$_{4-5}$MA–DBCO's LCST was 2 °C lower than the P(EG)$_{4-5}$MA HP and 6–8 °C higher than P(EG)$_{4-5}$MA–AZs. Therefore, the increased hydrophobic content from DBCO did not substantially influence P(EG)$_{4-5}$MA's temperature-dependent solubility, indicating a DBCO composition greater than 5 mol% is required to influence P(EG)$_{4-5}$MA's LCST. Due to larger PEG side chains, P(EG)$_{8-9}$MA copolymers did not exhibit an aqueous LCST (Fig. S21C†) when heated to 65 °C.[31] Copolymer LCSTs will also predict hydrogel fouling properties as copolymers with LCSTs near or above body temperature will maintain their low-fouling properties; hydrogels are fouling at temperatures above their LCSTs due to increased hydrophobic interactions with proteins.[32]

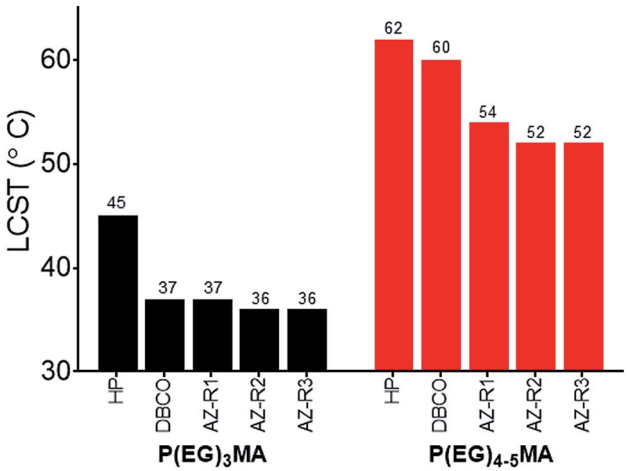

Fig. 2 P(EG)$_3$MA and P(EG)$_{4-5}$MA copolymer LCSTs. LCSTs (cloud points) of P(EG)$_3$MA and P(EG)$_{4-5}$MA homopolymers (HP) and AZ/DBCO copolymers (25 g L^{-1} in PBS) were determined by measuring solution turbidity at 600 nm as a function of temperature. LCSTs were defined as the lowest temperature that increased turbidity. No LCST was observed for P(EG)$_{8-9}$MA copolymers.

Table 1 P(EG)$_x$MA–APMA M_n, $Đ$ and composition

Polymer	M_n[a] (kDa)	$Đ$[a]	APMA[b] mol%
P(EG)$_3$MA–APMA	33.5	1.35	2
P(EG)$_{4-5}$MA–APMA	30.7	1.11	5
P(EG)$_{8-9}$MA–APMA	36.8	1.18	10

[a] M_n and $Đ$ determined by GPC calibrated with PEG standards. [b] APMA mol% determined *via* ^{1}H NMR.

3.2 ^{1}H NMR kinetic analysis of P(EG)$_x$MA–AZ carbamate degradation

To probe the influence of PEG M_W on carbamate degradation kinetics, ^{1}H NMR spectra of P(EG)$_x$MA–AZ copolymers with the 4-chlorophenyl sulfone EWG (P(EG)$_x$MA–AZ–R3) were acquired in real time for 3 h in borate buffer at pH 9.3, which increased reactions rates for efficient NMR analysis. Degradation was monitored by peak intensity changes of aromatic protons in 4-chlorophenyl sulfone, which is cleaved from the polymer upon hydrolysis. Over the course of the 3 h experiment, time-dependent losses in signal intensity were observed for polymer bound 4-chlorophenyl sulfone (aromatic protons, 7.8–8.1 ppm) and intensity gains for cleaved 4-chlorophenyl sulfone (aromatic protons, dashed box, sharp doublet, ≤7.8 ppm; Fig. 3A–C).

The degradation rate of P(EG)$_x$MA–AZ–R3 copolymers were dependent on the PEG M_W. P(EG)$_{8-9}$MA–AZ–R3 degraded immediately due to its higher solubility (LCST > 65 °C; Fig. 3D). In contrast, P(EG)$_{4-5}$MA–AZ–R3 exhibited a lag phase (~0.6 h) with no detectable degradation followed by a degradation rate similar to P(EG)$_{8-9}$MA–AZ–R3 (slopes of

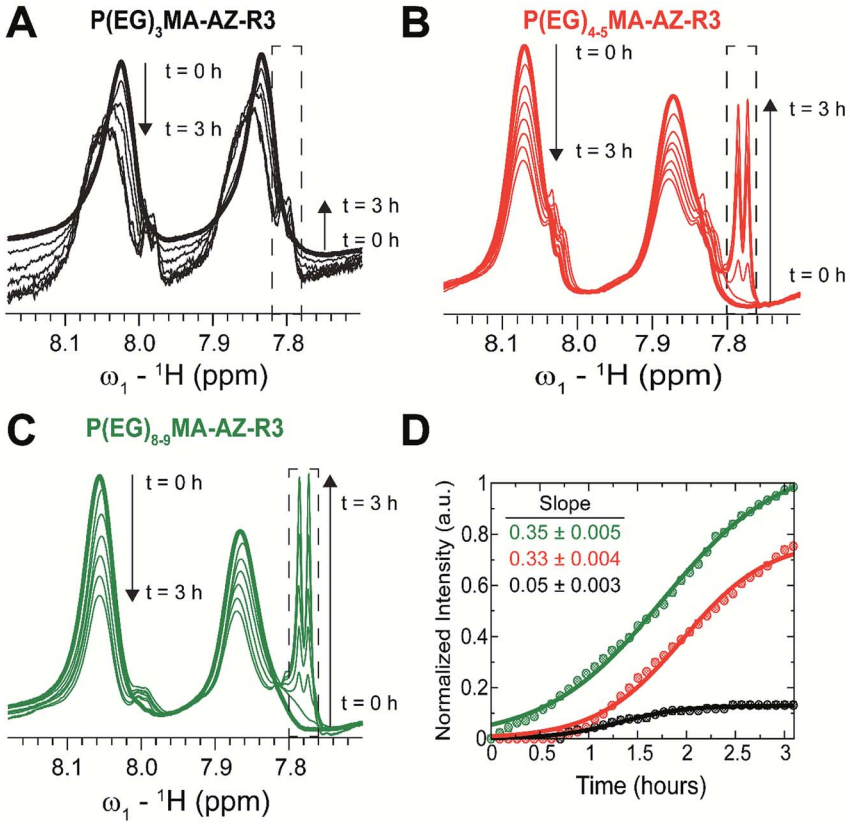

Fig. 3 ^{1}H NMR kinetic analysis of P(EG)$_x$MA–AZ–R3 copolymer crosslinker degradation at pH 9.3 and 37 °C. Upon base-catalysed degradation, 4-chlorophenyl sulfone is cleaved from the polymer resulting in the loss in signal intensity between 7.8–8.1 (two broad peaks) and appearance of a sharp doublet (≤7.8 ppm, dashed box). The rate of (A) P(EG)$_3$MA–AZ–R3, (B) P(EG)$_{4-5}$MA–AZ–R3, and (C) P(EG)$_{8-9}$MA–AZ–R3 degradation was followed over 3 h. (D) Degradation profiles as probed by changes in intensity of 4-chlorophenyl sulfone's aromatic protons. All intensities were normalized to the intensity of the P(EG)$_{8-9}$MA decomposition signature peak (dashed box) at the end of the 3 h period. Slopes were determined by linear regression of the normalized intensities; slopes were computed from 0 to 1 h for P(EG)$_{8-9}$–AZ–R3 and from ~0.6 to 1.6 h for P(EG)$_3$MA–AZ–R3 and P(EG)$_{4-5}$MA–AZ–R3.

0.33 and 0.35, respectively; Fig. 3D). The biphasic degradation profile of P(EG)$_{4-5}$MA–AZ–R3 is a function of polymer solubility over time; the cleavage of hydrophobic 4-chlorophenyl sulfone increases P(EG)$_{4-5}$MA–AZ–R3 solubility. Only minor P(EG)$_3$MA–AZ–R3 degradation was observed over the 3 h time period (Fig. 3A and D) because of its lower solubility at 37 °C, which is supported by LCST data (Fig. 2 and S22A†). From P(EG)$_{4-5}$MA–AZ–R3 data, we can conclude that PEG M_W mainly influences initial degradation rates.

3.3 Cytotoxicity of P(EG)$_x$MA copolymers

All P(EG)$_x$MA copolymers were non-cytotoxic according to NIH 3T3 fibroblast cell viability assays (Fig. 4). Cells were cultured in DMEM/F12 media with 10% calf bovine serum (CBS) in the presence of a single copolymer (1 mg mL^{-1}). After 24 h, cell viability was determined using the PrestoBlue assay and compared to a positive control, cells cultured without polymer. All copolymer conditions were indistinguishable from the positive control, indicating copolymers are non-cytotoxic and suitable for hydrogel fabrication.

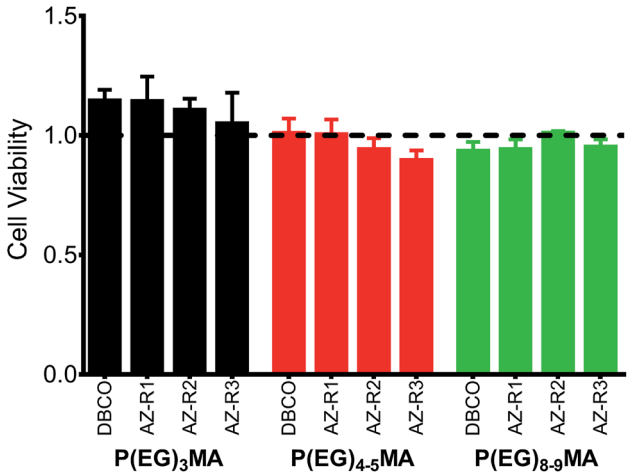

Fig. 4 P(EG)$_x$MA copolymers are non-cytotoxic. NIH 3T3 fibroblasts were cultured in the presence of 1 mg mL^{-1} of each copolymer for 24 h. Cell viability was assessed by the PrestoBlue assay and normalized to cells cultured in the absence of polymer (positive control, dashed line). No significant difference (p < 0.05) was observed between all polymer conditions and the positive control (mean + standard deviation, n = 3).

3.4 Hydrogel gelation and characterization

Non-degradable P(EG)$_x$MA–AZ copolymers were mixed with corresponding P(EG)$_x$MA–DBCO copolymers for *in situ* gelation and characterization of hydrogel crosslink density, swelling and protein fouling. Hydrogels were prepared by mixing equal volumes of corresponding azide and DBCO copolymer solutions (5 wt% in PBS) for strain-promoted alkyne–azide cycloaddition (SPAAC) crosslinking, and gelation times were determined by gravitational flow analysis (Fig. 5A); gelation time increased with larger PEGs, which limits crosslinking rates due to sterics.[33]

To study the influence of polymer hydration (PEG M_W) on hydrogel degradation, all P(EG)$_x$MA hydrogels (P(EG)$_3$MA, P(EG)$_{4-5}$MA, and P(EG)$_{8-9}$MA) required similar crosslink densities. The density of hydrogel crosslinks (μmol per g of polymer) was determined by quantifying DBCO consumption after SPAAC crosslinking (Table 2); unreacted DBCO absorbs light at 309 nm with an extinction coefficient of 12 000 M^{-1} cm^{-1}.[34] To achieve P(EG)$_x$MA hydrogels with similar crosslink densities, copolymer precursors with different AZ and DBCO mole fractions were required due to unique crosslinking kinetics. P(EG)$_3$MA, P(EG)$_{4-5}$MA, and P(EG)$_{8-9}$MA required crosslinker mole fractions of 2, 5, and 10 mol%, respectively, to yield hydrogels with similar crosslink densities (47–52 μmol of crosslinks per g of polymer).

Table 2 Hydrogel crosslink density

Hydrogel (5 wt%)	μmol of crosslinks per g of polymer[a]
P(EG)$_3$MA	52
P(EG)$_{4-5}$MA	47
P(EG)$_{8-9}$MA	48

[a] Determined 22 h after copolymer mixing.

Crosslink densities were determined by measuring unreacted DBCO concentrations (absorbance at 309 nm) after an overnight incubation to ensure maximum crosslinking. To calculate hydrogel background absorbance, all gels were subsequently exposed to excess sodium azide to consume remaining DBCOs.[35]

To compare hydration of P(EG)$_x$MA hydrogels, hydrogel cloud points and swelling ratios were determined. The cloud points of non-degradable (R1) and degradable (R2, Fig. 5B, S23A and B†) P(EG)$_3$MA and P(EG)$_{4-5}$MA hydrogels were similar to their corresponding P(EG)$_x$MA–AZ and P(EG)$_x$MA–DBCO copolymers; P(EG)$_3$MA and P(EG)$_{4-5}$MA hydrogels had cloud points of 36 and 54 °C, respectively. As expected from P(EG)$_{8-9}$MA copolymer LCSTs, P(EG)$_{8-9}$MA gels did not exhibit a cloud point (Fig. S23C†). In agreement with hydrogel cloud points, the equilibrium swelling ratio of P(EG)$_x$MA hydrogels

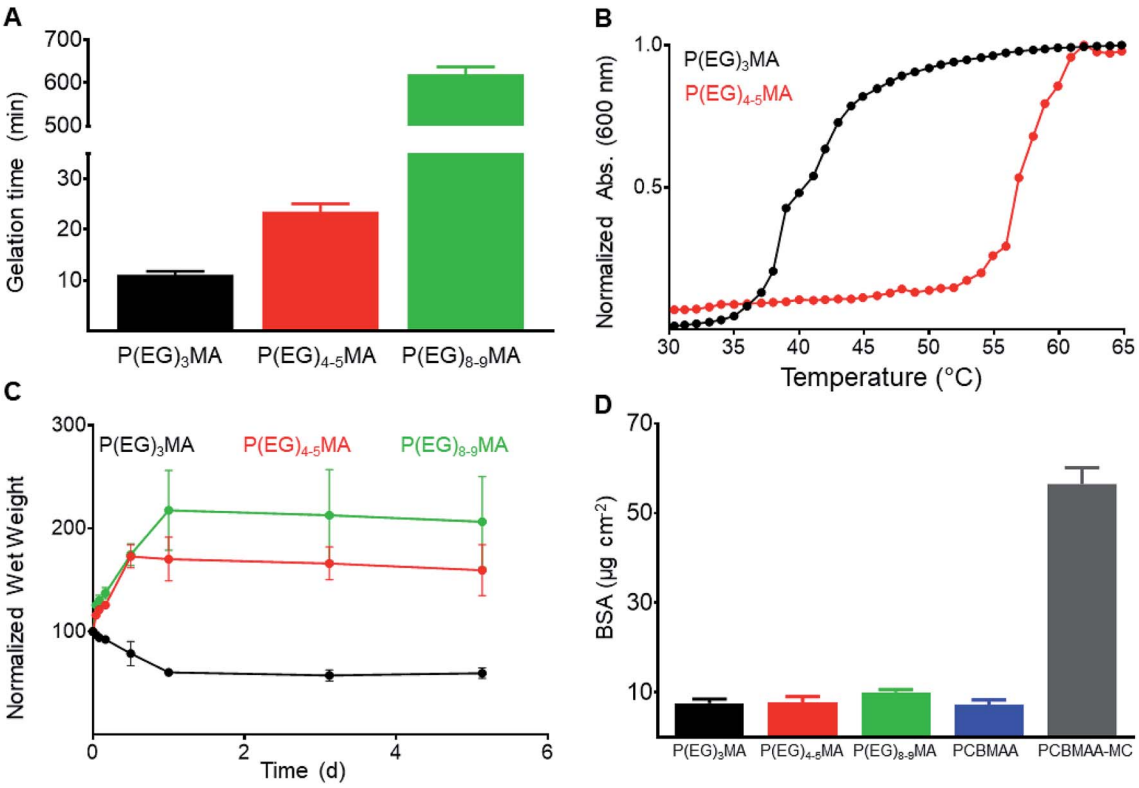

Fig. 5 Characterization of non-degradable P(EG)$_x$MA hydrogels: gelation time, hydration and protein fouling. (A) Hydrogel (5 wt%) gelation time, determined by gravitational flow analysis (mean + standard deviation, $n = 6$). (B) Cloud point of P(EG)$_3$MA and P(EG)$_{4-5}$MA hydrogels (5 wt% in PBS) defined as the onset of turbidity (600 nm). No cloud point was observed for P(EG)$_{8-9}$MA gels. (C) Equilibrium swelling of non-degradable gels. After overnight gelation, hydrogels (5 wt%) were submerged in PBS and their wet weight was determined at specified time points (mean ± standard deviation, $n = 3$). (D) Adsorbed fluorescent BSA (μg cm^{-2}) on hydrogel surfaces compared to low-fouling PCBMAA gels (6 mol% AZ/DBCO) and fouling PCBMAA–MC gels (mean + standard deviation, $n = 3$).

increased with greater PEG M_W (Fig. 5C). P(EG)$_3$MA gels incubated at 37 °C shrunk by expelling ~40% of their initial water content, due to the promotion of polymer–polymer interactions at temperatures near its cloud point (36 °C). P(EG)$_{4-5}$MA (cloud point 54 °C) and P(EG)$_{8-9}$MA hydrogels swelled to ~160 and 200%, respectively, of their initial wet weight.

To ensure P(EG)$_x$MA retained their low-fouling properties, we quantified the non-specific adsorption of fluorescent BSA to hydrogel surfaces. Non-degradable hydrogels were incubated in 0.5 mg mL^{-1} fluorescent BSA solutions for 2 h and rinsed with PBS. Adsorbed fluorescent BSA was extracted from the hydrogels with a sodium dodecyl sulfate (SDS) solution for quantification.[22] All gels bound between 5 and 10 μg cm^{-2} of fluorescent BSA, similar to other low-fouling hydrogels[22] (Fig. 5D). PCBMAA hydrogels with 6 mol% AZ/DBCO content and PCBMAA gels with 0.5 wt% methylcellulose (PCBMAA–MC) were included as controls; PCBMAA gels remain non-fouling with AZ/DBCO content below 10 mol%[36] and PCBMAA–MC gels non-specifically absorbed BSA due to MC hydrophobic interactions. PCBMAA and PCBMAA–MC non-specifically bound ~5 and 60 μg cm^{-2} of BSA, respectively. Therefore, all P(EG)$_x$MA gels remained non-fouling towards BSA.

3.5 Tunable degradation of P(EG)$_x$MA hydrogels

By developing a library of P(EG)$_x$MA–AZ and P(EG)$_x$MA–DBCO copolymers with R2 and R3 crosslinkers, we were able to easily achieve hydrogel degradation over 6 to 52 d (Fig. 6). Degradation rates were controlled by polymer hydration (P(EG)$_3$MA, P(EG)$_{4-5}$MA, and P(EG)$_{8-9}$MA) and the acidity of the crosslinker's β-hydrogen by exchanging EWG groups (4-methylphenyl sulfone or 4-chlorophenyl sulfone). Because PEG M_W influenced degradation rates (Fig. 3), each crosslinker (R2 or R3) yielded three different hydrogel degradation profiles. Hydrogels with higher PEG M_Ws degraded faster due to greater polymer solvation and initial degradation rates, as demonstrated by hydrogel swelling (Fig. 5C) and ^{1}H NMR kinetic studies (Fig. 3). For example, P(EG)$_3$MA–R3, P(EG)$_{4-5}$MA–R3 and P(EG)$_{8-9}$MA–R3 gels degraded over 52, 13 and 6 d, respectively (Fig. 6). As expected, P(EG)$_x$MA hydrogels degraded faster with crosslinks containing the stronger EWG (4-chlorophenyl sulfone, R3).

P(EG)$_3$MA hydrogels, which shrunk over time (Fig. 5C), produced the slowest degradation profiles (Fig. 6A and D). P(EG)$_3$MA–R3 gels degraded over 52 d, 4-fold slower than P(EG)$_{4-5}$MA–R3 gels. Therefore, PEG M_W has a significant impact on hydrogel degradation timeframes. Interestingly, P(EG)$_3$MA–R2 gels remained intact for >120 d. We expect P(EG)$_3$MA–R2 gels to eventually degrade because P(EG)$_3$MA–R3 gels degraded, which indicates that crosslink deprotonation and cleavage occur in P(EG)$_3$MA gels. Therefore, the design of P(EG)$_3$MA gels that degrade over 6 to >120 d may be possible using the developed copolymer library. Because

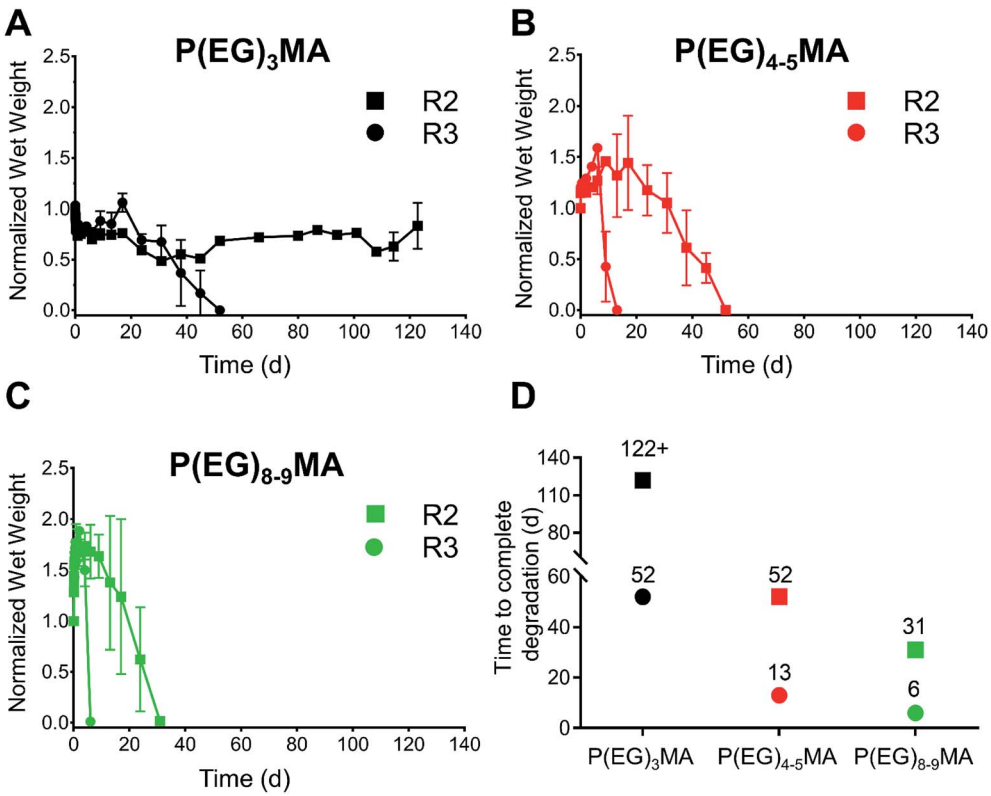

Fig. 6 Tunable degradation of P(EG)$_x$MA hydrogels at pH 7.4. The combination of different P(EG)$_x$MA copolymers with R2 or R3 crosslinkers yields low-fouling hydrogels that degrade over 6 to 52 d. The degradation of (A) P(EG)$_3$MA, (B) P(EG)$_{4-5}$MA, and (C) P(EG)$_{8-9}$MA hydrogels (100 μL, 5 wt%) with R2 (4-methylphenyl sulfone) or R3 (4-chlorophenyl sulfone) crosslinkers was followed over time in pH 7.4 PBS at 37 °C (mean ± standard deviation, $n = 3$). (D) Illustration summarizing time required for complete degradation of each hydrogel.

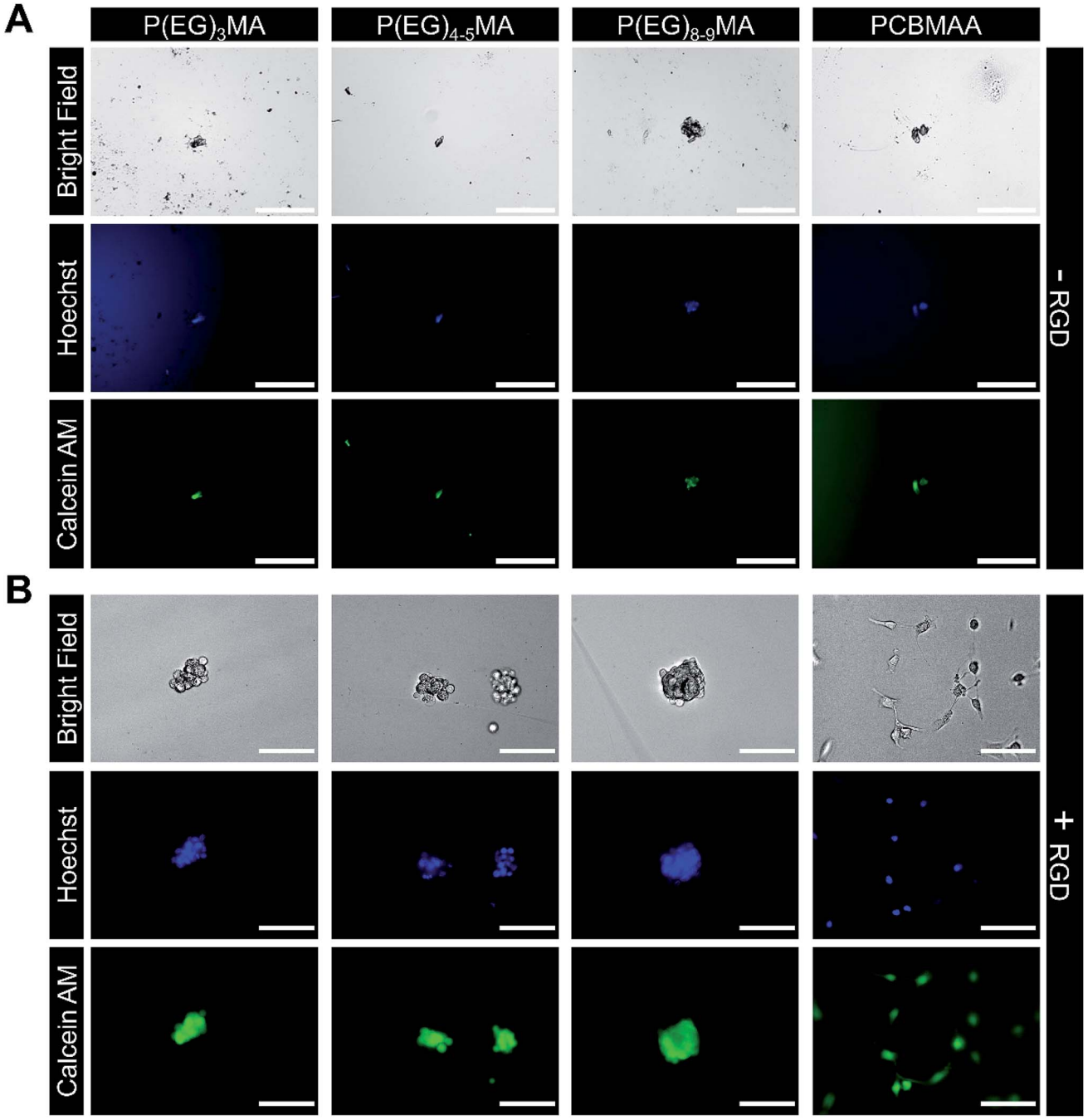

Fig. 7 Cell adhesion to P(EG)$_x$MA and PCBMAA hydrogels with and without immobilized RGD. Fibroblasts were seeded on gel surfaces and incubated for 24 h in DMEM/F12 with 10% CBS, gels were gently washed to remove non-adhered cells and stained with Calcein AM and Hoechst. (A) No cell adhesion was observed on P(EG)$_x$MA and PCBMAA gel surfaces without RGD. (B) Only a small number of cell clusters were observed on the surface of all P(EG)$_x$MA gels modified with RGD, indicating limited cell adhesion. In contrast, cell attachment and spreading on PCBMAA gels modified with RGD was similar to TCP controls (scale bars: 200 μm for −RGD and 100 μm for +RGD micrographs; $n = 3$). Micrographs of cells adhered to TCP are presented in Fig. S25.†

P(EG)$_3$MA–R3 and P(EG)$_{4-5}$MA–R2 gels both degraded over 52 d, low-fouling P(EG)$_x$MA hydrogels can be tuned to degrade over 6, 13, 31 or 52 d from a library of 6 P(EG)$_x$MA copolymers: (1) P(EG)$_{4-5}$MA–AZ–R2; (2) P(EG)$_{4-5}$MA–AZ–R3; (3) P(EG)$_{4-5}$MA–DBCO; (4) P(EG)$_{8-9}$MA–AZ–R2; (5) P(EG)$_{8-9}$MA–AZ–R3; and, (6) P(EG)$_{8-9}$MA–DBCO.

3.6 P(EG)$_x$MA gels are non-cell adhesive

Non-specific binding of cells to hydrogels can impede drug and cell delivery. To demonstrate P(EG)$_x$MA gels are resistant to non-specific cell adhesion, non-degradable P(EG)$_x$MA gels were exposed to fibroblasts in 10% CBS in DMEM/F12 media. After 24 h, gel surfaces were gently washed with PBS to remove non-

adhered cells. After staining with Calcein AM and Hoechst, micrographs of cells on gel surfaces were collected. No adhered cells were detected on any P(EG)$_x$MA gel (Fig. 7A), indicating the gels are low-fouling towards cells. PCBMAA gels formed through *in situ* PCBMAA–AZ and PCBMAA–DBCO (6 mol% AZ/DBCO) crosslinking were included as controls; PCBMAA gels are known to resist non-specific cell binding[36] (Fig. 7A).

P(EG)$_x$MA gels modified with RGD cell adhesion peptides demonstrated limited cell adhesion, indicating P(EG)$_x$MA gels also hindered integrin mediated adhesion. Excess DBCO groups in P(EG)$_x$MA gels were modified with an RGD-AZ peptide; the reaction was monitored by decreasing DBCO absorbance (309 nm; data not shown). Fibroblasts were seeded on hydrogel surfaces and incubated for 24 h. Cells were then stained with Calcein AM and Hoechst gels, gently washed with PBS to remove non-adhered cells, and gel surfaces were imaged. Only small cell clusters were observed on RGD modified P(EG)$_x$MA gels indicating weak RGD mediated cell–hydrogel interactions (Fig. 7B). In contrast, cells adhered to RGD modified PCBMAA gels (Fig. 7B) with morphologies similar to cells on tissue culture plastic (TCP; Fig. S25†). PCBMAA polymers are known to promote protein–ligand interactions,[37] whereas the PEG pendant groups in P(EG)$_x$MA may hinder protein–ligand complexation; PEG polymers are known to decrease enzymatic activity.[37] Because all hydrogels contained a large excess of DBCO groups (>100 nmol cm^{-2} on the surface) for RGD immobilization, all hydrogel surfaces had sufficient RGD for cell adhesion (>1 fmol cm^{-2}).[38] Therefore, P(EG)$_x$MA gels are ideal for applications that require minimal protein and cell binding.

For some stem cell delivery applications, degradable hydrogels functionalized with adhesive peptide have been shown to improve cell survival.[39] Therefore, we incorporated the two crosslinkers (R2 and R3) into PCBMAA hydrogels (Scheme S1†), which degraded over 13 and 52 d (Fig. S24C†). Due to the high solubility of PCBMAA copolymers, the rate of PCBMAA hydrogel degradation was expected to be similar to P(EG)$_{8-9}$MA gels, which degraded over 6 and 31 d. The slower degradation rate was attributed to PCBMAA's greater crosslink density than P(EG)$_{8-9}$MA gels (128 *vs.* 48 μmol g of polymer). Therefore, the PCBMAA hydrogel can be used for short- and long-term applications that require bioactive hydrogels.

3.7 Further discussion

The developed degradation mechanism for low-fouling P(EG)$_x$MA gels tunes the deprotonation rate of the carbamate crosslinker independently from endogenous triggers by changing EWGs and PEG M_W, which provides a method to reliably achieve different hydrogel degradation timeframes. All components, except for released CO_2, remain covalently bound to degraded non-cytotoxic copolymers, we therefore expect minimal *in vivo* toxicity for future applications. Moreover, all degradation timeframes (6, 13, 31, and 52 d) can be achieved from highly soluble P(EG)$_{4-5}$MA and P(EG)$_{8-9}$MA copolymers (LCSTs > physiological temperature) and will therefore remain soluble after hydrogel degradation to further improve biocompatibility.

Controlled degradation of hydrogels is important for drug and cell delivery. For example, the sustained release of antibody checkpoint inhibitors for ~1 week from degradable poly(vinyl alcohol) hydrogels improved survival in a melanoma mouse model by 50% over intravenous injections.[40] Adoptive cell therapies are improved by creating a local cell depot with injectable hydrogels that degrade to allow for cell egress. Hydrogels have been shown to improve transplantation efficiency of neural stem cells[41] and T cell infiltration[42] into tumors for cancer immunotherapies. The ability to control hydrogel degradation will improve adoptive cell therapies by controlling the rate of cell egress from the hydrogel into surrounding tissue. Therefore, we demonstrated that encapsulated fibroblasts in P(EG)$_x$MA gels retained high viability to ensure the crosslinking mechanism is not cytotoxic (Fig. S26†); SPAAC crosslinking has previously been demonstrated to be non-cytotoxic.[43] To avoid unwanted adverse events (*e.g.* FBR), low-fouling hydrogels that degrade over several days to weeks are required, such as those developed here.

The degradation rate of P(EG)$_x$MA gels will influence both drug and cell delivery. For the developed P(EG)$_x$MA gels, cells seeded on the surface of RGD modified hydrogels did not migrate into the gel, indicating hydrogel pore sizes are submicron and prevent cell migration. Therefore, the degradation rate of the P(EG)$_x$MA gels will be the main determinant for cell delivery rates. However, hydrogel degradation will not be required for drug efflux because P(EG)$_x$MA gels with similar and higher crosslink densities have previously been demonstrated to release proteins for drug delivery applications.[44] Although, faster degradation rates will increase rates of drug release.

4. Conclusions

The developed 6-member P(EG)$_x$MA copolymer library allows for the rapid fabrication of low-fouling hydrogels that degrade over 6 to 52 d, which will be useful for short- and long-term drug and cell delivery applications. Furthermore, P(EG)$_3$MA–R2 may result in hydrogels that degrade over >120 d. The combination of tunable base-catalyzed crosslink degradation and P(EG)$_x$MA hydration provides a simple method to rapidly tune degradation rates. Given that the non-cytotoxic P(EG)$_x$MA gels remained low-fouling towards proteins and cells, it is expected that they will help mitigate adverse immune responses (*e.g.* FBR) upon implantation. Interestingly, P(EG)$_x$MA gels modified with RGD remained non-cell adhesive by preventing integrin mediated adhesion. The established low-fouling P(EG)$_x$MA hydrogel library that easily achieves different degradation timeframes will expedite the establishment of drug and cell delivery therapies.

Conflicts of interest

There are no conflicts of interest to declare.

Acknowledgements

This work was supported by the Natural Sciences and Engineering Research Council (NSERC: 2015-05429, 506209-16), Canada Foundation for Innovation: John R. Evans Leaders Fund (CFI-JELF: 34107), Ontario Research Fund – Research Infrastructure (ORF-RI: 34107), and McMaster University. We would also like to thank Dr Alex Adronov and Stuart McNelles for donation of NHS-DBCO.

References

1 J. M. Anderson, A. Rodriguez and D. T. Chang, *Semin. Immunol.*, 2008, **20**, 86–100.
2 R. Klopfleisch and F. Jung, *J. Biomed. Mater. Res., Part A*, 2017, **105**, 927–940.
3 W. Chen, B. C. Yung, Z. Qian and X. Chen, *Adv. Drug Delivery Rev.*, 2018, **127**, 20–34.
4 C. Leng, S. Sun, K. Zhang, S. Jiang and Z. Chen, *Acta Biomater.*, 2016, **40**, 6–15.
5 W. Feng, S. Zhu, K. Ishihara and J. L. Brash, *Biointerphases*, 2006, **1**, 50–60.
6 W. Feng, X. Gao, G. McClung, S. Zhu, K. Ishihara and J. L. Brash, *Acta Biomater.*, 2011, **7**, 3692–3699.
7 W. Yang, H. Xue, W. Li, J. Zhang and S. Jiang, *Langmuir*, 2009, **25**, 11911–11916.
8 L. Zhang, Z. Cao, T. Bai, L. Carr, J. R. Ella-Menye, C. Irvin, B. D. Ratner and S. Jiang, *Nat. Biotechnol.*, 2013, **31**, 553–556.
9 A. Singh and N. A. Peppas, *Adv. Mater.*, 2014, **26**, 6530–6541.
10 C. Bastiancich, P. Danhier, V. Préat and F. Danhier, *J. Controlled Release*, 2016, **243**, 29–42.
11 M. Norouzi, B. Nazari and D. W. Miller, *Drug Discovery Today*, 2016, **21**, 1835–1849.
12 S. V. Bharambe, A. B. Darekar and R. B. Saudagar, *Int. J. Pharm. Technol.*, 2013, **5**, 2764–2786.
13 N. Gerwin, C. Hops and A. Lucke, *Adv. Drug Delivery Rev.*, 2006, **58**, 226–242.
14 M. F. Rai and C. T. Pham, *Curr. Opin. Pharmacol.*, 2018, **40**, 67–73.
15 S. G. Schwartz, I. U. Scott, H. W. Flynn and M. W. Stewart, *Expert Opin. Drug Delivery*, 2013, **11**, 61–68.
16 V. Huynh and R. G. Wylie, *Angew. Chem., Int. Ed.*, 2018, **57**, 3406–3410.
17 J. Li and D. J. Mooney, *Nat. Rev. Mater.*, 2016, **1**, 16071.
18 L. Zhang, H. Xue, Z. Cao, A. Keefe, J. Wang and S. Jiang, *Biomaterials*, 2011, **32**, 4604–4608.
19 H. W. Chien, X. Xu, J. R. Ella-Menye, W. B. Tsai and S. Jiang, *Langmuir*, 2012, **28**, 17778–17784.
20 P. Jain, H.-C. C. Hung, B. Li, J. Ma, D. Dong, X. Lin, A. Sinclair, P. Zhang, M. B. O'Kelly, L. Niu and S. Jiang, *Langmuir*, 2019, **35**, 1864–1871.
21 G. Cheng, F. Cheng, H. Wang, H. Wu and F. Xu, *RSC Adv.*, 2016, **6**, 30862–30866.
22 D. Dong, J. Li, M. Cui, J. Wang, Y. Zhou, L. Luo, Y. Wei, L. Ye, H. Sun and F. Yao, *ACS Appl. Mater. Interfaces*, 2016, **8**, 4442–4455.
23 E. Bakaic, N. M. B. Smeets, M. Badv, M. Dodd, O. Barrigar, E. Siebers, M. Lawlor, H. Sheardown and T. Hoare, *ACS Biomater. Sci. Eng.*, 2018, **4**, 3713–3725.
24 I. Urosev, E. Bakaic, R. J. Alsop, M. C. Rheinstädter and T. Hoare, *J. Mater. Chem. B*, 2016, **4**, 6541–6551.
25 H.-W. W. Chien, W.-B. B. Tsai and S. Jiang, *Biomaterials*, 2012, **33**, 5706–5712.
26 J. Leijten, J. Seo, K. Yue, G. Trujillo-de Santiago, A. Tamayol, G. U. Ruiz-Esparza, S. R. Shin, R. Sharifi, I. Noshadi, M. M. Álvarez, Y. S. Zhang and A. Khademhosseini, *Mater. Sci. Eng., R*, 2017, **119**, 1–35.
27 D. V. Santi, R. Reid, E. L. Schneider, G. W. Ashley and L. Robinson, *Proc. Natl. Acad. Sci. U. S. A.*, 2012, **109**, 6211–6216.
28 G. W. Ashley, J. Henise, R. Reid and D. V Santi, *Proc. Natl. Acad. Sci. U. S. A.*, 2013, **110**, 2318–2323.
29 Z. Cui, B. H. Lee, C. Pauken and B. L. Vernon, *J. Biomed. Mater. Res., Part A*, 2011, **98**, 159–166.
30 S. M. Hodgson, E. Bakaic, S. A. Stewart, T. Hoare and A. Adronov, *Biomacromolecules*, 2016, **17**, 1093–1100.
31 J. F. Lutz, *J. Polym. Sci. Part A: Polym. Chem.*, 2008, **46**, 3459–3470.
32 B. Yang, C. Wang, Y. Zhang, L. Ye, Y. Qian, Y. Shu, J. Wang, J. Li and F. Yao, *Polym. Chem.*, 2015, **6**, 3431.
33 N. M. B. Smeets, E. Bakaic, M. Patenaude and T. Hoare, *Acta Biomater.*, 2014, **10**, 4143–4155.
34 N. Kotagiri, A. Nehorai, Z. Li, S. Achilefu, X. Xu and S. Mondal, *Bioconjugate Chem.*, 2014, **25**, 1272–1281.
35 M. Bjerknes, H. Cheng, C. D. McNitt and V. V. Popik, *Bioconjugate Chem.*, 2017, **28**, 1560–1565.
36 V. Huynh, A. Jesmer, M. M. Shoaib and R. G. Wylie, *Langmuir*, 2019, **35**, 1631–1641.
37 A. J. Keefe and S. Jiang, *Nat. Chem.*, 2012, **4**, 59–63.
38 S. P. Massia and J. A. Hubbell, *J. Cell Biol.*, 1991, **114**, 1089–1100.
39 S. S. Ho, K. C. Murphy, B. Y. K. Binder, C. B. Vissers and J. K. Leach, *Stem Cells Transl. Med.*, 2016, **5**, 773–781.
40 C. Wang, J. Wang, X. Zhang, S. Yu, D. Wen, Q. Hu, Y. Ye, H. Bomba, X. Hu, Z. Liu, G. Dotti and Z. Gu, *Sci. Transl. Med.*, 2018, **10**, eaan3682.
41 L. R. Nih, S. T. Carmichael and T. Segura, *Curr. Opin. Biotechnol.*, 2016, **40**, 155–163.
42 S. B. Stephan, A. M. Taber, I. Jileaeva, E. P. Pegues, C. L. Sentman and M. T. Stephan, *Nat. Biotechnol.*, 2015, **33**, 97–101.
43 S.-S. Han, H. Y. Yoon, J. Y. Yhee, M. O. Cho, H.-E. Shim, J.-E. Jeong, D.-E. Lee, K. Kim, H. Guim, J. H. Lee, K. M. Huh and S.-W. Kang, *Polym. Chem.*, 2018, **9**, 20–27.
44 E. Bakaic, N. M. B. Smeets, H. Dorrington and T. Hoare, *RSC Adv.*, 2015, **5**, 33364–33376.

